

AIR-WATER FLOW IN A VERTICAL PIPE WITH SUDDEN CHANGES OF SUPERFICIAL WATER VELOCITY

Eckhard Krepper¹, Horst-Michael Prasser

Institute of Safety Research, Research Centre Rossendorf, Dresden, D-01314, Germany

E.Krepper@fz-rossendorf.de, H.M.Prasser@fz-rossendorf.de

Thomas Frank

ANSYS CFX Germany, Staudenfeldweg 12, D-83624 Otterfing, Germany

Thomas.Frank@ansys.com

ABSTRACT

For further model development and the validation of CFD codes for two-phase flow applications experiments were carried out with a sudden change of the superficial velocity of water in a vertical pipe of 51.2 mm diameter. Measurements of the cross sectional gas volume fraction distributions were taken by two wire-mesh sensors (24x24 points, 2500 Hz) mounted in a short distance (16 mm) behind each other. This sensor assembly was placed 3030 mm downstream of the gas injection. The change of the superficial water velocity was jump-like reduced and in a second series of tests jump-like increased. The tests enable the observation of the restructuring process of bubbly flow between two steady state conditions. The experimental results for tests showing a monodisperse bubble size distribution were compared to CFD calculations using the code CFX-5. Applying the two fluid approach, the momentum interaction between the liquid and gas phase was considered. For the experimental conditions of dispersed bubbly flows without or with neglectable bubble coalescence & breakup the main flow features observed in the experiments could be reproduced qualitatively and quantitatively by the numerical simulation. Further research will be undertaken for the investigation of flow regime transition from gaseous phase volume fraction wall peak to core peak dominated flows. Further investigations will also include compressibility effects for the disperse bubbly phase.

1. INTRODUCTION

For two-phase CFD the correct models of the momentum exchange between gas and liquid are of crucial importance. Additional to the interphase drag the non-drag forces like lift, wall lubrication and turbulent dispersion forces have to be taken into account, where the latter lead to the finally observable gas volume fraction distributions in the measurement cross section at $z=3.03\text{m}$ due to their lateral balance perpendicular to the main flow direction. One way to validate the performance of these models is to compare CFD calculations with measurements. In many cases, this was done for experiments that were carried out under steady state conditions, because instrumentation capable in revealing information about the flow structure like gas fraction and velocity profiles, bubble size distributions, gas-liquid interface (e.g. multiple-tip optical fibre probes) require long measuring periods.

The application of wire-mesh sensors allowed to decrease the measuring time significantly (Prasser et al., 1998). Statistically reliable profiles and bubble size distributions can be obtained within a few seconds. For example, this advantage was used to characterise the flow structure and the instantaneous drift parameters during flashing in experiments related to the start-up of boiling water reactors by Manera et al. (2003, 2004).

¹ Corresponding author

The main idea for the experiments presented in this paper was to measure transient profiles and bubble size distributions under unsteady conditions generated in a vertical upward gas-liquid flow by a quick change of the liquid superficial velocity (Noack, 2003). It turned out, that a special value of these tests consists in the following: the effect of the acceleration or, respectively, deceleration of two-phase mixture can be directly studied, since a certain portion of fluid mixture formed before the perturbation arrives at the measuring position still after the flow rate change. In this portion of fluid mixture, the bubble size distribution remains constant. In this way, the effect on radial void fraction profiles and on the drift velocity can be studied independently from changing bubble sizes.

2. THE EXPERIMENTS

2.1. Experimental Test Facility

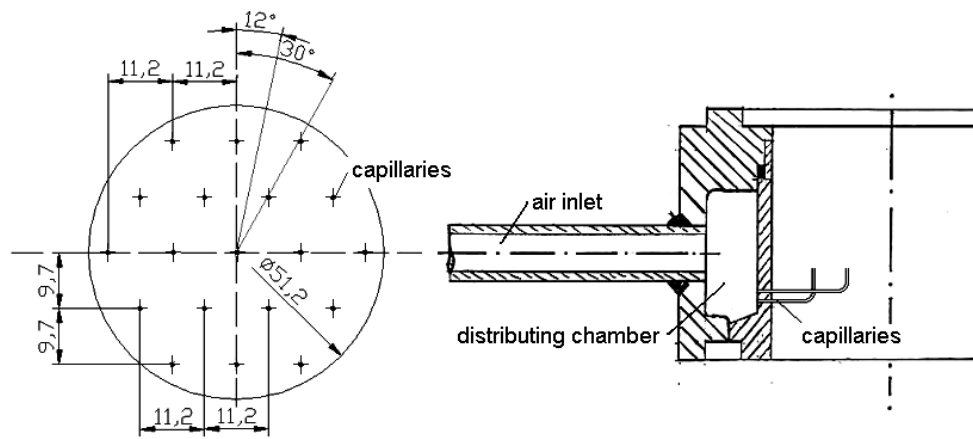


Figure 1: Gas injection device



Figure 2: Flap of the fast acting valve, left: original flap, right: perforation

The experiments were carried out at the MTLloop test facility previously used for instrumentation development and flow map studies (Krüsenberg et al., 2000). To produce a sudden change of the superficial water velocity, a butterfly valve with a pneumatic activation was used (Noack, 2003). The total time of the valve action was about 0.2 s. By perforating the flap of the valve (Fig. 2) it was achieved, that a rapid closure did not reduce the water flow rate to zero, but caused a jump-like

reduction of the liquid flow rate. The valve was located about 1.5 m upstream of the gas injection. In a second series of tests a jump-like increase of the water flow rate was studied, which was induced by a sudden opening of the valve.

2.2. Instrumentation

Measurements were taken by two wire-mesh sensors (Fig. 3, Prasser et al., 1998) mounted in a distance of 16 mm behind each other. Each disposed of a grid of 24x24 measuring points in the cross section (some of them in the corners being outside the circular cross section of the pipe). This sensor assembly was placed 3030 mm downstream of the gas injection. Beside the mesh sensors, the facility was equipped with thermocouples and flow meters for both liquid and gas.

The wire-mesh sensor is sensible to the electrical conductivity of the fluid. The data evaluation starts from the transformation of the instantaneously measured electrical signals into local instantaneous gas fractions. For this, the instantaneous conductivity value at each measuring point is related to the value recorded for plain water. The result is a matrix of local instantaneous volumetric gas fractions $\epsilon_{i,j,k}$, where k is the number of the current measurement and i, j are the indexes of to the location in the sensor plane.

The sensors were used to record signal sequences with a frequency of 2500 frames per second over a total period of 17 s. The valve was activated 1 s after the start of the data acquisition, i.e. during a period of 1 s the undisturbed initial steady state was still present.

The data of the two sensors are used to calculate cross-section averaged gas fractions as well as radial gas fraction profiles. The profiles were derived from the wire-mesh sensor data by performing an averaging over radial ring-shaped domains (see Prasser, Lucas, Krepper, 2002). The averaging time interval was set to 0.25 s in order to characterise the transient changes in the profiles. For a better statistic reliability of the data, an ensemble-averaging was performed over 10 repetitions of the experiment, carried out under identical boundary conditions.

Gas velocity profiles were obtained by a point-to-point cross-correlation of all available measuring points of the two sensors (Prasser, 2000), calculated over time intervals of 0.25 s. Again, in order to increase statistical reliability, an ensemble averaging was performed over 10 realizations of the transient process. In this way, a matrixes of 24x24 velocity values were calculated, that were afterwards transformed into radial velocity profiles, again by averaging over radial ring-shaped domains.

Bubble sizes were calculated using the algorithm published by Prasser et al. (2001). The radial velocity profiles obtained by cross-correlation were used to calculate the extensions of the bubbles in vertical directions from their passage time through the measuring plane of the sensor. For each bubble, the time-averaged gas velocity measured at the location of its centre of mass was used.

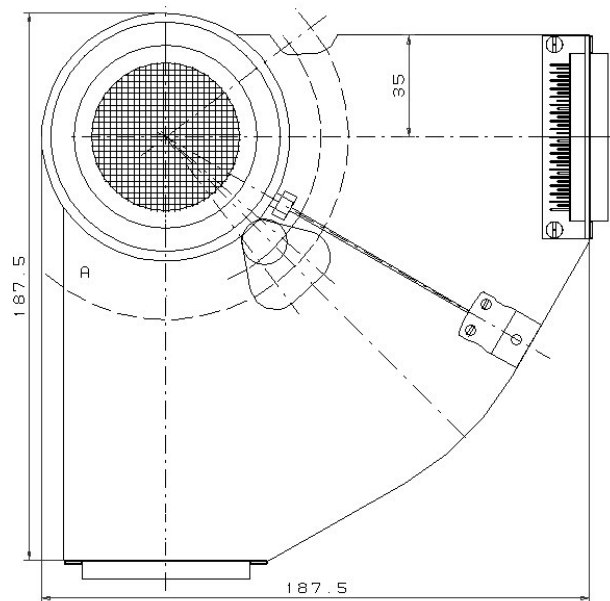


Figure 3: Wire-mesh sensor with 24x24 measuring points (wires: stainless steel, diameter: 120 μm ; lateral pitch = resolution: 2 mm; axial distance between wire planes: 1.7 mm; measuring frequency: 2500 Hz)

3. CFD CALCULATIONS

The experiment was simulated with the CFD-code CFX-5.7. using the two fluid approach. The two fluid model (Ishii, 1975 and 1984) is an Eulerian-Eulerian time averaged model. Two sets of governing equations, continuity and momentum equations are solved for either phase and their interactions are modelled using interface transfer terms.

The liquid was modelled as a continuous fluid, whereas the gas was regarded as disperse bubbles. The drag between bubbles and liquid was modelled according to Grace (1976). The gaseous phase was assumed to consist of bubbles of a uniform size. In the blind pre-test calculation presented here, the bubble diameter was set to 4 mm.

For the liquid a turbulence shear stress (SST) model was applied in accordance to Menter (1994). The influence of the gas bubbles on the liquid was modelled using Sato's (1975) eddy viscosity model for bubble induced turbulence.

Besides the drag forces, representing the flow resistance, the non drag forces have to be modelled to simulate the correct flow structure. Namely the lift force, the turbulent dispersion and the wall force have to be considered. In the following expressions the forces for the gaseous dispersed phase are given.

The lift force was calculated according to Zun (1980):

$$\vec{F}_{lift} = -C_{lift} \rho_w (\vec{w}_G - \vec{w}_w) \times rot \vec{w}_w \quad (1)$$

with the gas and liquid velocity w_G and w_w and the liquid density ρ_w . Tomiyama (1998) has performed extensive investigations of the lift force coefficient C_{lift} . For an air-water two-phase flow he has found a changing sign of C_{lift} depending on the bubble size diameter at about $d_b = 5.8$ mm:

$$C_{lift} = \begin{cases} \min[0.288 \tanh(0.121 Re), f(Eo_d)] & Eo_d < 4 \\ f(Eo_d) & \text{for } 4 < Eo_d < 10 \\ -0.27 & Eo_d > 10 \end{cases} \quad (2)$$

$$\text{with } f(Eo_d) = 0.00105 Eo_d^3 - 0.0159 Eo_d^2 - 0.0204 Eo_d + 0.474$$

The coefficient depends on the modified Eötvös number:

$$Eo_d = \frac{g(\rho_l - \rho_g)d_b^2}{\sigma}$$

with d_b as the the equivalent bubble diameter regarding the bubble volume.

The wall force pushes the bubbles away from the wall and can be considered according to

$$\vec{F}_w = -C_w \alpha \rho_w \left[(\vec{w}_G - \vec{w}_w) - ((\vec{w}_G - \vec{w}_w) \cdot \vec{n}_r) \vec{n}_r \right]^2 \vec{n}_r \quad (3)$$

with

$$C_w = \max \left\{ 0, \frac{C_{w1}}{d_b} + \frac{C_{w2}}{y} \right\} \quad (\text{Antal 1991}), \text{ respective}$$

$$C_w = C_{w3} \frac{d_b}{2} \left(\frac{1}{y^2} - \frac{1}{(D-y)^2} \right) \quad (\text{Tomiyama 1998})$$

with \vec{n}_r as the normal vector to the wall, d_b as the bubble size diameter, w_{rel} as the velocity difference between the phases and a as the gas volume fraction. The force is dependent on the distance to the wall y . Antal (1991) proposes an inverse proportionality to y , whereas Tomiyama (1998) proposes for a tube of a diameter D an inverse quadratic proportionality to y .

The applied turbulent dispersion force is based on the Favre average of the interfacial drag force (see Burns et al. 2004, Frank et al. 2004) and is calculated for a two phase flow according to

$$\vec{F}_{Disp} = D_{G,L} A_{G,L} \frac{v_{W,t}}{\sigma_L} \left(\frac{\nabla \overline{\alpha_L}}{\alpha_L} - \frac{\nabla \overline{\alpha_G}}{\alpha_G} \right) \quad (4)$$

with $D_{G,L}$ as the phase drag coefficient, $A_{G,L}$ the interfacial area density, $v_{W,t}$ the water turbulence viscosity including the contribution from Sato's eddy viscosity model and σ_L the turbulent Schmidt Number.

These non drag forces were implemented in CFX-5 and are available since the code version CFX-5.7 (see Shi et al. 2004).

The tube was modelled by a 60° sector with two symmetry planes. The fluid injection was modelled by an INLET boundary condition from below simulating a turbulent radial velocity profile. During the transient the velocity value was changed depending on the test. 0.5 m above the inlet the gas was injected by point sources simulating the inlet nozzles according to the specified air superficial velocity. At the top of the vertical tube a pressure boundary condition was defined. The computational grid consisted of 32000 hexahedral cells.

4. TEST CONDITIONS

Tests were performed for different combinations of the initial superficial velocities of water $J_{L,1}$ and air J_G (Figs. 4 and 5). After 1 s of steady-state recording, the valve was activated in the desired direction and new specific flow rate of the water ($J_{L,2}$) established. The liquid superficial velocity was changed approximately by factor 3 (see subscripts of Figs. 4 and 5). The total measuring time of the mesh sensors was set to 17 s. In all experiments, the temperature was kept constant at 30 °C. Desalinated water with a conductivity of less than 1 μS/cm was used.

At most of the tests conditions a pronounced wall peak of the radial gas fraction profile was formed both before and after the flow rate change. At higher gas and lower liquid flow rates a central peak was observed, sometimes a transition profile occurred, characterised by two maxima in the centre and close to the wall.

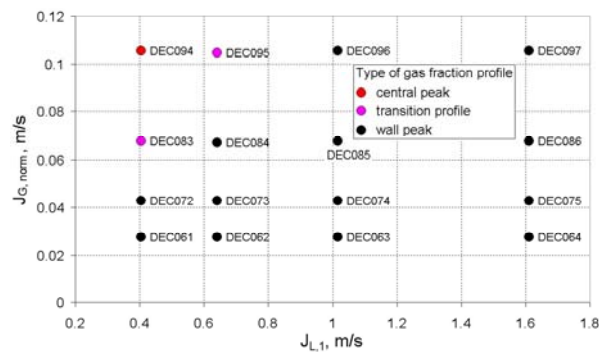


Figure 4: Matrix of initial conditions of the tests with sudden reduction of the liquid superficial velocity ($J_{L2}/J_{L1} = 0.28 \dots 0.36$)

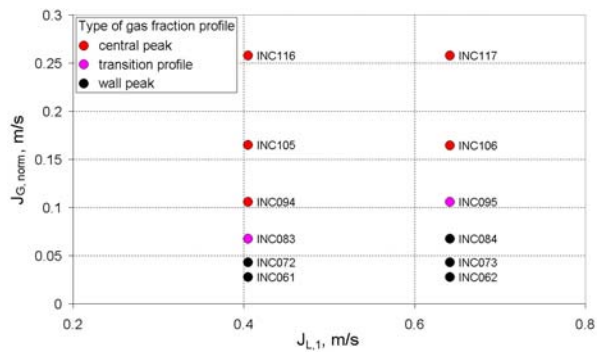


Figure 5: Matrix of initial conditions of the tests with sudden increase of the liquid superficial velocity ($J_{L2}/J_{L1} = 3.4 \dots 3.6$)

5. RESULTS OF THE EXPERIMENTS

As examples for sudden increase of the liquid flow rate the test INC61 and for sudden decrease the test DEC63 were considered here in detail. The time history of the cross-section averaged gas fractions measured by the first wire-mesh sensor is given in Fig. 6a for INC61 and in Fig. 6b for DEC63. The change of the liquid flow rate takes place at $t=0$ s. In all tests the process can be divided into three main stages, which are separated by transition periods. Stage 1 corresponds to the undisturbed flow before the flow rate change ($t<0$ s). In stage 2, a portion of two-phase mixture, that has still been generated at initial conditions, arrives at the sensor position at the new liquid velocity. Then, after the elapse of the total travelling time of the disturbance between gas injection and sensor, the flow regime transits to stage 3, which represents the final state (Fig 6a for $t>4$ s, Fig. 6b for $t>9$ s). Between the mentioned stages of established conditions transient processes characterized by acceleration or deceleration of the fluids are observed.

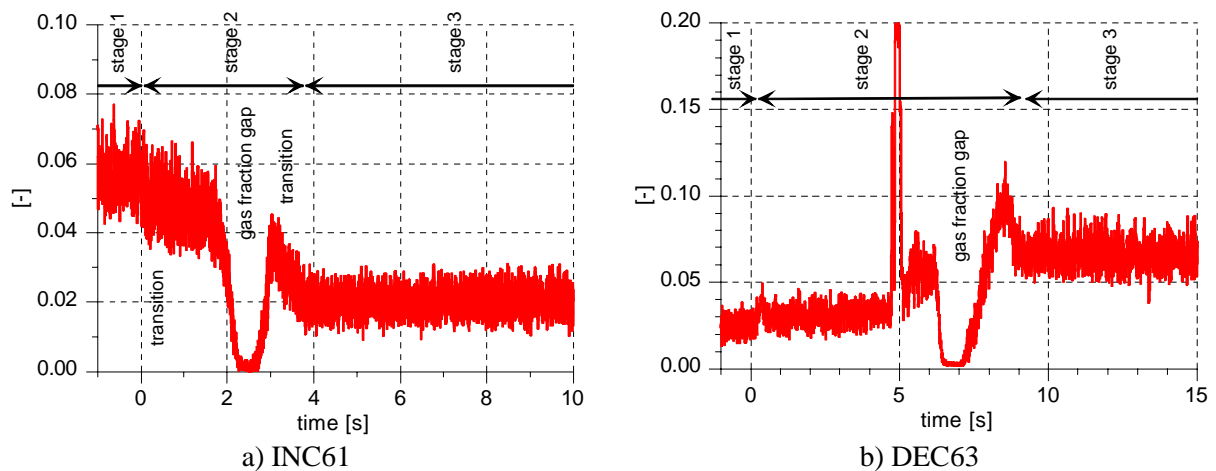


Figure 6: Time history of the cross-section averaged gas fraction at sensor 1 in a test

- a) with sudden increase of the liquid superficial velocity
(INC61, $J_G=0.0235$ m/s, $J_L=0.4048 \rightarrow 1.417$ m/s)
b) with sudden reduction of the liquid superficial velocity
(DEC63, $J_G=0.0235$ m/s, $J_L=1.067 \rightarrow 0.283$ m/s)

For a sudden increase respective decrease of the liquid superficial velocity, the cross section averaged gas fraction decreases respectively increases from stage 1 to stage 2 and from stage 2 to stage 3. The decrease respectively increase from the initial conditions to the final state is obvious, since the same gas flow rate is injected into a liquid flow with growing flow rate. Although, the decrease between phases 1 and 2 needs special attention.

The two-phase mixture in both stages has still been produced before the perturbation of the fluid flow rate under identical conditions at the gas injection device. Due to the comparatively low gas fractions, coalescence is practically absent. This is reflected by identical bubble size distributions before and after the perturbation (Fig. 7), which were found for all tests listed in Table 1. From this follows that the performed experiments allow to study the effect of a liquid velocity change on a swarm of bubbles of constant sizes.

The decreasing gas fraction for the increasing liquid velocity leads to a run away of the bubbles with the consequence of a gas fraction gap from 2.2 to 2.8 s (s. Fig. 6a). In the other case of decreasing liquid velocity the bubbles accumulate and form a Taylor bubble at $t=5$ s (s. Fig. 6b).

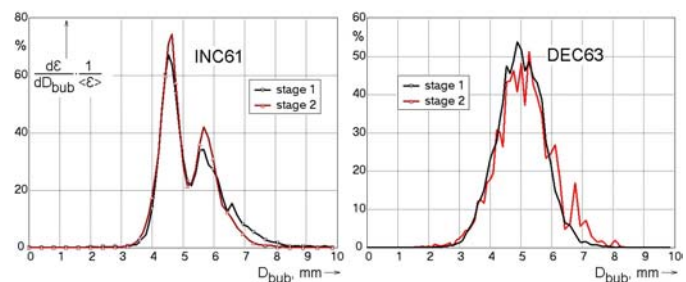


Figure 7: Bubble size distributions in stage 1 and stage 2 of the tests INC61 and DEC63

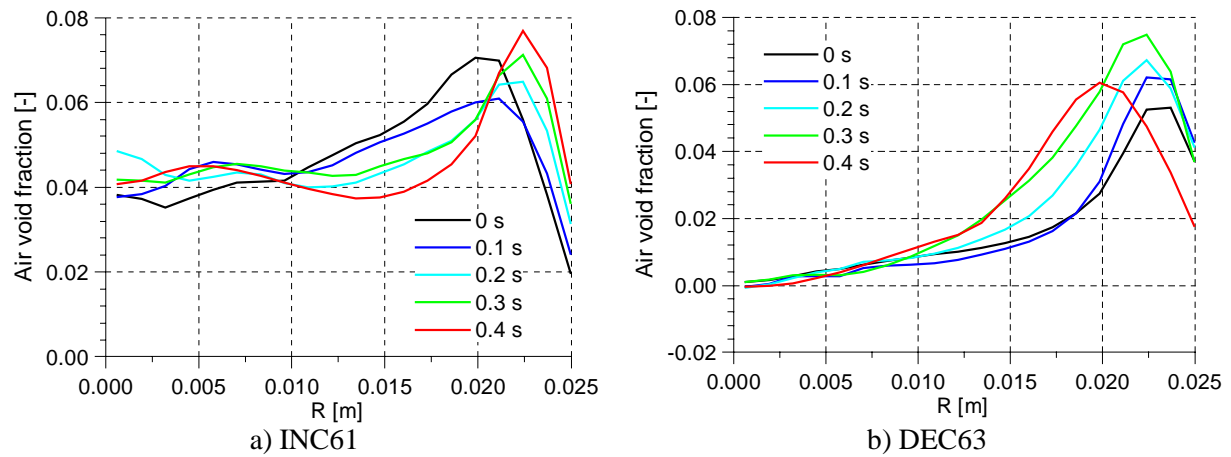


Figure 8: Measured radial gas fraction profiles at the transition from stage 1 to stage 2

Fig. 8 shows the changing gas fraction profiles 3m behind the gas injection immediately after the change of the liquid velocity.

6. RESULTS OF THE CALCULATIONS

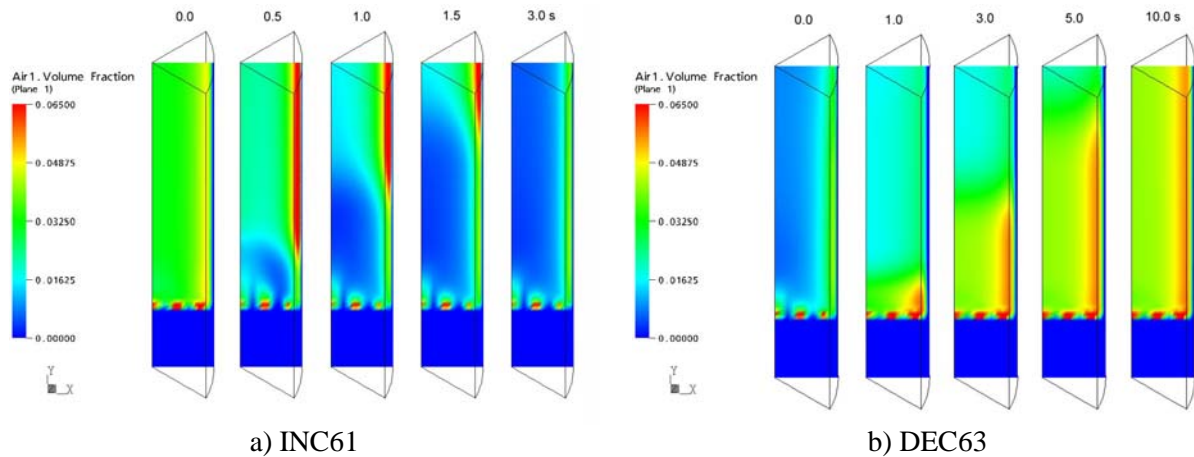


Figure 9: Void fraction distribution calculated by CFX-5.7 (axial compressed presentation)

Fig. 9 shows the calculated development of the void fraction distribution over the height of the pipe for both cases. The void fraction distribution in the pipe is at quasi-steady state at $T=0.0s$ (stage 1) and is instantaneously changed by the disturbance of the fluid flow rate. Afterwards the movement of the disturbance wave vertically upward in the pipe is clearly reproduced by the calculations, leading to a new quasi-steady state of the gas void fraction distribution, which is corresponding to the changed superficial water velocity at stage 3. Nevertheless the slight gas fraction changes and the gas fraction gap phenomena, which were observed in the experimentally measured and cross sectional averaged gas fractions during the transition stage 2, are not found in the calculations (s. Fig. 10 for the calculations, Fig 6 for the measurements).

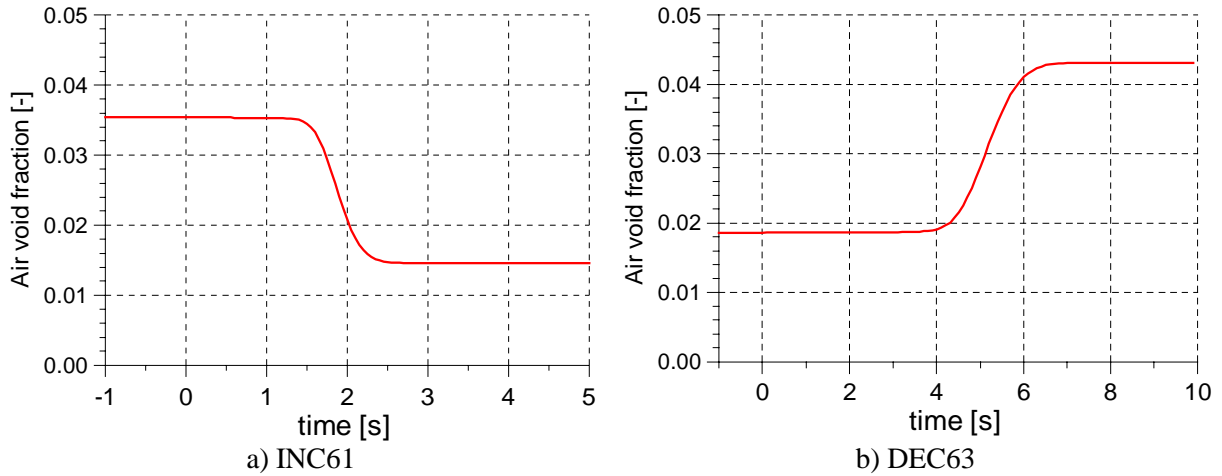


Figure 10: Calculated cross sectional averaged gas fraction at 3m behind the gas injection (compare Fig. 6)

Fig. 11 shows the time history of the gas and liquid superficial velocities at the sensor position (3m behind the gas injection). In the transition stage 2 the gas superficial velocity is increased (Fig. 11a) respectively decreased (Fig. 11b) since the same gas content is moving in this period with another velocity.

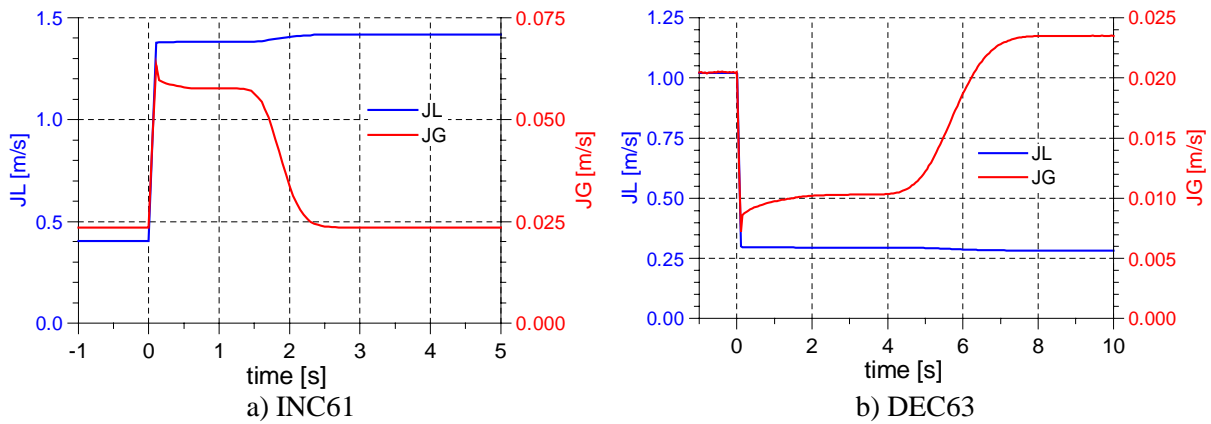


Figure 11: Calculated cross sectional averaged superficial velocities at 3m behind the gas injection

Figure 12 shows the changing gas profiles short after changing the water velocity. The profiles are calculated in good agreement to the experiments (see Fig 8 for the measurements).

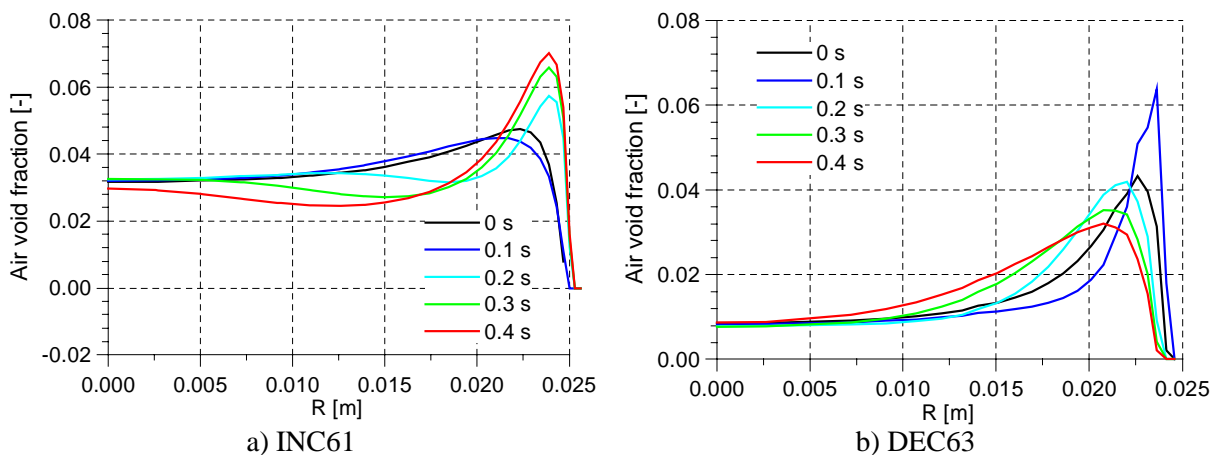


Figure 12: Calculated radial gas fraction profiles at the transition from stage 1 to stage 2 at 3m behind the gas injection (compare Fig. 8)

The initially observed wall peak gets closer to the wall, when the liquid velocity is increased (see Fig. 12a). This is caused by the lift force, that acts on the bubbles perpendicular to the main flow direction. It grows with increasing gradient of the liquid velocity, which itself grows with the absolute liquid velocity. In the consequence, the bubbles are shifted into a region, where the local liquid velocity related to the cross-section averaged velocity is lower. If we assume that the rise velocity of the bubbles relative to the water remains unchanged, this would lead to a decrease of the drift velocity and should therefore cause a growth of the gas fraction. In case of a sudden decrease of the liquid flow rate, similar effects with inverted tendencies were observed (see Fig. 12b).

The simulation enables the calculation of more complex values like the profile factor C_0 .

7. ACCURACY OF THE MEASUREMENTS

The measuring errors of the wire-mesh sensors have to be discussed with respect to different aspects. Due to the complexity of the interaction between gas bubbles and the electrode grids, errors are difficult to assess. The accuracy of the gas fractions was checked by comparing the wire-mesh data with gamma-transmission measurements and ultra-fast X-ray tomography. Especially the studies in an air-water flow in a vertical pipe using the ultra-fast X-ray tomograph of AIST Tsukuba, Japan (Misawa et al., 1998) delivered valuable information. A wire-mesh sensor was placed closely downstream of the measuring plane of the X-ray device. The cross-section averaged void fractions calculated directly from the radiation attenuation along the chords between X-ray tubes and detectors has shown a very good agreement between mesh sensor and the X-ray device (Prasser, Misawa, Tiseanu, submitted). In the bubble flow regime, which is of interest here, the deviation of the absolute cross-section averaged gas fractions is less than 1 %. This supports the correctness of the behaviour of the gas fraction found in our experiments.

Concerning the shape of the gas-liquid interface and the feed-back of the sensor to the flow experimental studies were performed at a transparent channel with a square cross section of 50 x 50 mm (Prasser et al., 2001). Electrode wires were directly fixed in small drillings in the acrylic glass walls of the channel and the interaction of bubbles with the wires was observed using a high speed video camera. It was found that bubbles are broken up when they come in contact with the wires. Nevertheless it was demonstrated that the sensor signal still represents the correct shape of the undisturbed bubbles with the accuracy given by the lateral pitch of the wires. The high-speed video sequences obtained at the transparent test channel mentioned above were also used to assess the volume of individual bubbles during their passage through the sensor plane. The calculated equivalent bubble diameters were compared to the bubble sizes measured by the wire-mesh sensor. At liquid velocities above 0.2 m/s individual bubble diameters measured by the two methods correspond within bands of ± 20 %.

The present experiments allow to compare bubble size distributions obtained by two wire-mesh sensors put behind each other. Typical examples are shown in Fig. 13. It was observed that the second sensor gives slightly decreased bubble sizes. This is due to the fragmentation caused by the first sensor. We have to keep in mind that the gas velocity profile obtained by cross-correlation is reflecting the situation between the two sensors, i.e. it corresponds to bubbles, that are smaller than those in the test section upstream of the sensors. However, the effect diminishes with growing liquid velocity. For this reason, the systematic error of the velocity measurement caused by the bubble fragmentation should decrease with growing superficial velocity, too. Since the highest drift velocities were observed at high superficial velocities, measuring errors to be anticipated due to bubble fragmentation are most likely not able to fake the observed effect.

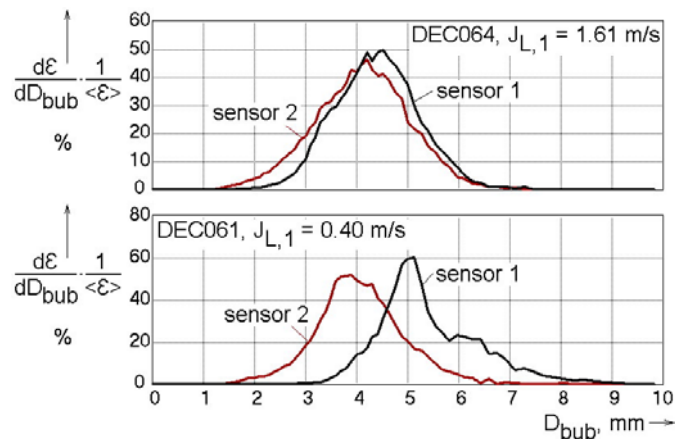


Figure 13: Comparison of the bubble size distributions measured by the first and the second wire-mesh sensor at different liquid flow rates (examples, stage 1 of the named experiments)

8. CONCLUSIONS

In the measurements a change of the cross-sectional averaged gas fraction during a sudden change of the liquid superficial velocity was found, which is in contradiction to the expected results and to the result of CFD calculations, when the change of the radial gas fraction profile is taken into account. A bubble size change can be excluded as a possible reason. It was found that drift velocities calculated from wire-mesh sensor signals are significantly greater than those predicted by the correlation of Zuber & Findlay (1965), if the total superficial velocity is greater than 0.75 m/s. Most of the existing drift-flux correlations do not predict a dependency of the drift velocity that is as strong as the observed effect. It was furthermore found that the increase of the pressure gradient cannot explain the effect.

On the other hand, the effect was confirmed by velocity profile measurements carried out by cross-correlating the signals of two sensors put behind each other. This is a second measuring method that is independent from the gas fraction measurements by the wire-mesh sensor. For this reason it is believed that the observed effects are real and not caused by systematic measuring errors. The reason of the observed increase of drift velocity is still unclear. Further investigations are necessary to confirm the findings, as well as to clarify the nature of the effect.

Furthermore, the data obtained by wire-mesh sensors in unsteady two-phase flow experiments offer the possibility to perform CFD code validation under highly transient conditions.

REFERENCES

- Antal S. P., R. T. Lahey J. E. Flaherty, 1991, Analysis of phase distribution in fully developed laminar bubbly two-phase flow, *Int. J. Multiphase Flow*, Vol. 17, 635-652
- Burns A.D., Frank T., Hamill I. and Shi, J.-M. 2004. The favre averaged drag model for turbulence dispersion in Eulerian multi-phase flows. *5th Int. Conf. on Multiphase Flow, ICMF'2004*, Yokohama, Japan.
- Frank Th. Shi J. Burns A.D. 2004. Validation of Eulerian multiphase flow models for nuclear reactor safety applications, *3rd International Symposium on Two-phase Flow Modelling and Instrumentation*, Pisa, 22.-24. Sept. 2004
- Grace J.R., T. Wairegi, and T.H. Nguyen, 1976, Shapes and velocities of simple drops and bubbles moving freely through immiscible liquids, *Trans. Inst. Chem. Eng.*, Vol. 54, pp. 167
- Ishii, M. and K. Mishima, 1984, Two fluid model and hydrodynamic constitutive relations, *Nuclear Engineering and Design*, Vol. 82, pp. 107-126..
- Krüssenberg, A.K., H.-M. Prasser, A. Schaffrath, 2000, A New Criterion for the Bubble Slug Transition in Vertical Tubes, *Kerntechnik* 65/1 (2000) 7-13
- Manera A. H.-M. Prasser, T. H. J. J. van der Hagen, 2003, Suitability of Drift-flux models, void-fraction evolution and 3D flow pattern visualization during stationary and transient flashing flow in a vertical pipe, *The 10th International Topical Meeting on Nuclear Reactor Thermal Hydraulics (NURETH-10)*, Seoul, Korea, October 5-9, 2003; conference-CD: A00108.
- Manera A., H.-M. Prasser, D. Lucas, T. H. J. J. van der Hagen, 2004, Study of bubble size distributions and three-dimensional flow pattern visualisation in stationary and transient upwards flashing flow by means of wire-mesh sensors, *3rd International Symposium on Two-phase Flow Modelling and Instrumentation*, Pisa, 22.-24. Sept. 2004.
- Menter F.R., 1994, Two-equation eddy-viscosity turbulence models for engineering applications, *AIAA-Journal*, Vol. 32, No. 8.
- Misawa M., K. Ichikawa, N. Akai, M. Hori, K. Tamura, G. Matsui, 1998, Development of Fast X-ray CT System for Transient Two-Phase Flow Measurement, *Proc. 6th Int. Conf. Nucl. Eng.*, ICONE-6383, San Diego, USA, 1998.
- Noack R. 2003, Experimentelle Untersuchung von getriggerten Zweiphasenströmungen in einer vertikalen Rohrleitung, Forschungszentrum Rossendorf, Februar 2003, Praktikumsbericht.
- Prasser H.-M., A. Böttger, J. Zschau, 1998, A new electrode-mesh tomograph for gas-liquid flows, *Flow Measurement and Instrumentation*, 9 (1998), 111-119.
- Prasser H.-M., 2000, High-speed measurement of the void fraction distribution in ducts by wire-mesh sensors, *International Meeting on Reactor Noise*, Oct. 11-13, 2000, Athens, Greece, proc. on CD-ROM, paper_7_1.doc.
- Prasser, H.-M., D. Scholz, C. Zippe, 2001, Bubble size measurement using wire-mesh sensors, *Flow Measurement and Instrumentation*, 12/4, pp.299-312, 2001.
- Prasser H.-M., E. Krepper, D. Lucas, 2002, Evolution of the two-phase flow in a vertical tube - decomposition of gas fraction profiles according to bubble size classes using wire-mesh sensors, *International Journal of Thermal Sciences*, 41 (2002) 17-28.

- Prasser H.-M., M. Misawa, I. Tiseanu, Comparison between wire-mesh sensor and ultra-fast X-ray tomograph for an air-water flow in a vertical pipe, *Flow Measurement and Instrumentation*, Article in press
- Sato Y., K. and Sekoguchi, 1975, Liquid velocity distribution in two phase bubble flow, *Int. J. Multiphase Flow*, Vol. 2, pp. 79-95.
- Shi J.-M., Frank T., Krepper E., Lucas D., Rohde U., Prasser H.-M. 2004. Implementation and Validation of Non-Drag Interfacial Forces in CFX-5, ICMF-2004, Yokohama, Japan
- Tomiyaama A., 1998. Struggle with computational bubble dynamics. *Third International Conference on Multiphase Flow*, ICMF-1998, Lyon, France, June 8-12, 1998
- Zun I., 1980, The transverse migration of bubbles influenced by walls in vertical bubbly flow, *Int. J. Multiphase Flow*, Vol. 6, pp. 583-588